2006

Evaluation of Thermoacoustic Cycles for Cooling Applications

Insu Paek
Purdue University

James E. Braun
Purdue University

Luc Mongeau
Purdue University

Evaluation of Thermoacoustic Cycles for Cooling Applications

Insu Paek*, James E. Braun, and Luc Mongeau

Ray W. Herrick Laboratories, School of Mechanical Engineering, Purdue University
West Lafayette, Indiana, USA

*Phone: 765-494-2147, Fax: 765-494-0787, paek@purdue.edu

ABSTRACT

The most promising applications for thermoacoustic cooling are investigated from the perspective of the thermodynamic second law efficiency in this paper. A design optimization program interacting with the thermoacoustic simulation program known as DELTAE was developed. Then it was applied to two of the most common configurations for standing-wave thermoacoustic coolers in order to determine the best possible second law efficiencies for various temperature spans between hot-side and cold-side stack-end temperatures. It was found that the second law efficiency of thermoacoustic coolers increases with temperature span and reaches a maximum for temperature lifts around 80 °C. Analysis of the results and the losses clearly show that from an efficiency perspective, thermoacoustics performs well for refrigeration applications but poorly for both air-conditioning and cryogenic cooling. The second law efficiencies determined from measurements for various thermoacoustic coolers developed so far show a similar trend.

1. INTRODUCTION

Thermoacoustic cooling is a recent technology that has been proposed to obtain cooling energy from a high amplitude sound wave. Periodic compression and expansion of gas particles, combined with heat transfer within regions near boundaries, results in heat pumping cycles with environmentally benign working fluids (Swift, 2002). There is significant interest in thermoacoustic cooling systems because they possess a few possible advantages over other technologies. These advantages include the use of environmentally benign working fluids, simple design, continuous cooling capacity control, and possible quiet operation. There are, however, noteworthy technical challenges related to the design and construction of efficient, robust, economical thermoacoustic cooling systems. Most of the systems conceived to date require a stack and two sets of heat exchangers between the primary and the conditioned working fluids, which increases complexity and irreversibility (Swift, 2002). For standing-wave thermoacoustic coolers, it is difficult to achieve very large cooling capacities with a single device. Furthermore, thermoacoustic system performance is very sensitive to the choice of design parameters and should be optimized to achieve a reasonable efficiency (Minner *et al.*, 1997).

Efforts have been made to optimize the design of thermoacoustic coolers by improving stack geometry, gas mixture, thermal insulation, duct and cone diameters, and other parameters. An optimization scheme to achieve the best electroacoustic driver efficiency was developed by Wakeland (2000) using equivalent electrical circuit theory. An equation was derived to calculate electroacoustic efficiency from known driver parameters. Optimization of the stack spacing for maximum COP or for maximum cooling power was experimentally investigated by Tijani *et al.* (2002a). It was observed that a stack spacing about three times larger than the thermal penetration depth (see next section) is optimal for thermoacoustic refrigeration. Systematic investigations of the effects of the Prandtl number of the gas mixture used in thermoacoustic cooling were also performed (Tijani *et al*., 2002b). It was observed that the second law efficiency, defined as the ratio of coefficient of performance (COP) to Carnot COP (Moran and Shapiro, 2000), increases with decreasing Prandtl number.

There also have been studies aimed at the systematic design optimization of thermoacoustic coolers. Wetzel and Herman (1997) used a model based on the boundary layer approximation, and the short stack assumption to calculate the work flux and heat flux; they optimized the system by adjusting nineteen design variables to achieve the best COP. A similar design optimization method was used by Tijani (2001) to design the stack of a thermoacoustic cooler. Instead of using simplified work flux and heat flux equations, Minner *et al.* (1997)

developed a design optimization program that interacts with DELTAE using a C^{++} computer program. From a parametric study, they observed that the efficiency of thermoacoustic coolers is sensitive to stack length, position, mean pressure and gas mixture (Prandtl number), and less sensitive to the stack spacing.

The second law efficiency of prototypes developed so far has varied between about 10% and 20% for different prototypes and for different cooling temperatures. Thermoacoustic coolers with a relatively small temperature span have poor second law efficiency, lower than 10 % (see table 5). This implies that there may be a relationship between the best achievable second law efficiency and the temperature span. Such relationship would allow the most promising application of thermoacoustic cooling in terms of second law efficiency can be identified. This was the motivation of the study of the second law performance of thermoacoustic coolers presented in this paper.

The objective of the present study was to identify the most promising application area for thermoacoustic cooling in terms of operating temperatures. In order to accomplish this goal, an optimization tool was built to identify the designs that result in the best efficiency for a range of imposed operating temperatures. Results from the optimization study allowed the identification of the major loss mechanisms, which may help to improve component design.

2. DESIGN OPTIMIZATION

2.1 Program

The design optimization program, based on work from a previous study (Minner *et al.*, 1997), used a nonlinear function minimization routine based on successive multi-dimensional applications of a one-dimensional golden section search with parabolic interpolation (Mathews and Fink, 1999). The golden section search method evaluates the cost function at two different points within a specified interval or constraints. It narrows the range where the minimum of the cost function is located. Because it is a one-dimensional method, a sequential minimization of the cost function for selected design variables was performed.

During development and validation, a one-dimensional method and the Nelder-Mead simplex multi-dimensional method were used (Nelder and Mead, 1965). The latter is known to be robust because it uses a direct search and doesn't require first-order or second-order derivative information to locate the minimum of the cost function. However, as for other minimization methods, the simplex method is vulnerable to convergence at a local minimum (Nelder and Mead, 1965). Results from the multi-dimensional, Nelder-Mead simplex method were found to be slightly less accurate than those from successive, one-dimensional optimization method. The latter approach was therefore used for the final analysis.

The design optimization program written in MATLAB minimizes the cost function given as

$$F_{\text{cost}} = -COPR(D1_n),\ n = 1, 2, 3, ..., N, \tag{1}$$

or

$$F_{\text{cost}} = -\eta_{dr}(D2_m),\ m = 1, 2, 3, ..., M. \tag{2}$$

In Eqs. (1) and (2), F_{cost} is the cost function, *COPR* is the second law efficiency, η_{dr} is the electroacoustic conversion efficiency of the driver, and $D1_n$, and $D2_{\text{m}}$ are the vectors of design variables having *N and M* dimensions, respectively. As mentioned earlier, *COPR* is defined as (Moran and Shapiro, 2000)

$$COPR = \frac{COP}{COP_{Carnot}}, \tag{3}$$

where *COP* is the coefficient of performance and COP_{Carnot} is the reversible *COP* given by

$$COP_{Carnot} = \frac{T_c}{\Delta T}. \tag{4}$$

In Eq. (4), T_c is the cold-side heat reservoir temperature and ΔT is the temperature difference between the hot-side heat reservoir and the cold-side heat reservoir. In this study, the hot and cold-side stack end temperatures were used as the hot and cold heat reservoir temperatures, respectively to evaluate the reversible *COP*.

The *COP* used in Eq. (3) is the ratio of cold heat exchanger heat transfer rate (cooling rate) and the thermoacoustic power provided by the driver. The electroacoustic conversion efficiency, η_{dr}, used in Eq. (2) is defined as

$$\eta_{dr} = \frac{\dot{W}_{ac}}{\dot{W}_e}, \tag{5}$$

where, $\dot{W}_{ac}$ is the acoustic power from the driver, and $\dot{W}_e$ is the electrical power input to the driver. The negative signs in Eqs. (1) and (2) are to facilitate the maximization of *COPR* and η_{dr}. The combined golden section search and parabolic method maximizes the second law efficiency with a series of *N* one-dimensional optimizations and maximizes the driver efficiency with a series of *M* one-dimensional optimizations. The coupled design variables were sequentially varied to locate the optimal points in each one-dimensional optimization. *N*+*M* sequential optimizations formed one set of optimizations. In order to consider coupling between the design variables, one set of the sequential one-dimensional optimizations was repeated until the relative variations of the cost functions, -*COPR* and -η_{dr}, were less than 0.1 % and 1 %, respectively. No constraints on the design variables were imposed.

The optimization program requires results obtained from DELTAE, a thermoacoustic simulation program commonly used to model thermoacoustic coolers (Ward and Swift, 1994). Numerical stability and convergence must be ensured for all cases encountered during the optimization process. Since DELTAE is based on a shooting method, it fails to converge when numerical solutions are too far from the initial guesses. In order to avoid this situation, upper and lower bounds for design variables were used for each iteration of the optimization to keep the change in design variables smaller than 10% of the values determined in the previous iteration.

A flowchart of the main optimization program and its subroutine is shown in Fig. 1. The design variables are first read. DELTAE is initialized. Upper and lower bounds for design variables are established, and subroutines are called for each one-dimensional optimization. There are separate subroutines for each design variable. New trial values of the selected design variable are written to the DELTAE input file. DELTAE is then used to obtain model predictions for *COPR* and η_{dr}, written in a DELTAE output file. This process is repeated until the cost function is minimized. Other subroutines are then called sequentially by the main program to optimize the remaining design variables until all design variables are optimal. This process constitutes one iteration of the overall optimization scheme. After each iteration, the relative change of the cost function (-*COPR* and -η_{dr}) is calculated for the last iteration. The process is terminated if changes are smaller than 0.1 % and 1 %, respectively.

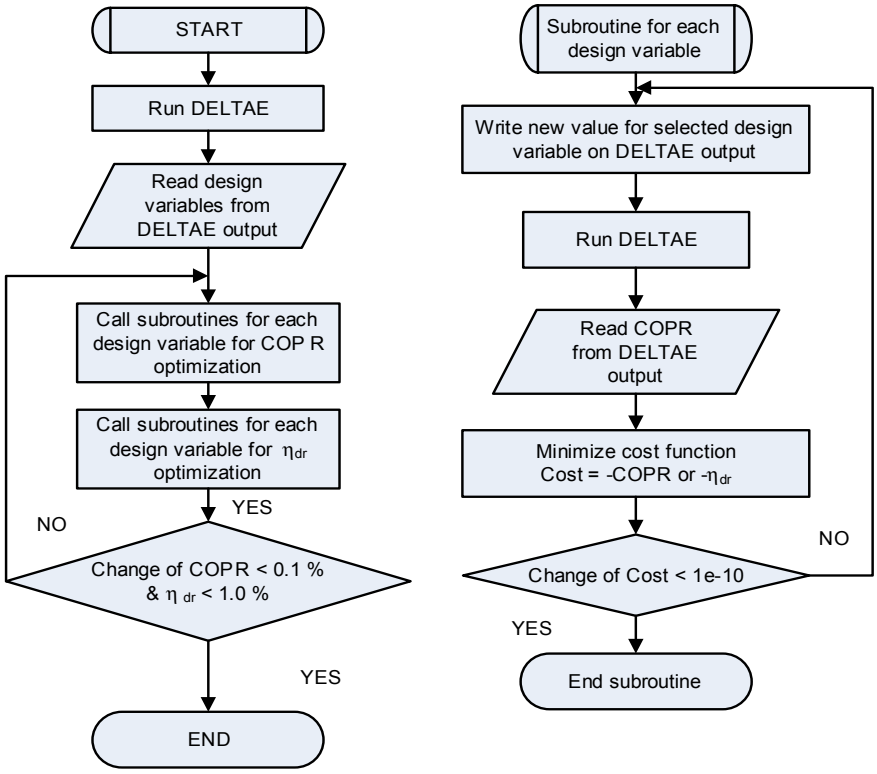

Figure 1: Flow chart for optimization program. The main program is on the left, and its subroutine is on the right.

2.2 Design Variables

Two similar configurations were used for the design optimization. Hofler's configuration is a Helmholtz resonator. The Purdue prototype configuration is a half-wavelength resonator. Design variables were chosen based on practical issues such as feasibility, cost, and fabrication. The stack spacing and porosity, for example, are not easily modified. Changes in heat exchanger dimensions would require new heat exchangers. Therefore these variables were excluded from the design variables. The selected design variables for Hofler's configuration, as shown in Fig. 2, include the length of Duct$_1$ (DL_1), the length and area of the stack (SL and SA), the length and area of duct$_2$ (DL_2 and DA_2), the length and final area of the horn (CL and CA), the Helmholtz resonator volume (HV), and the piston area (PA). All design variables were optimized for the best second law efficiency with the exception of the piston area (PA). The piston area was determined independently to achieve optimal driver electroacoustic conversion efficiency.

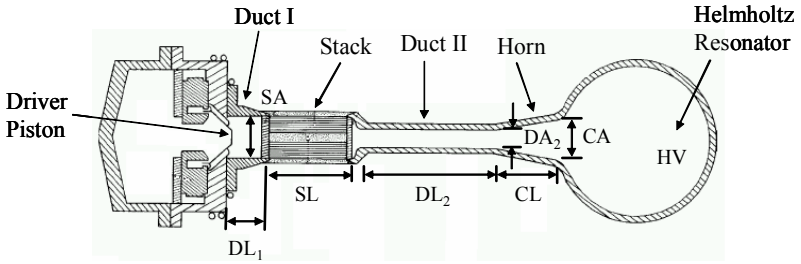

Figure 2: Design variables for Hofler's prototype.

The selected design variables for the Purdue prototype, as shown in Fig. 3, were the length of Cone 1 (CL_1), the length, and area of the stack (SL, SA), length of cone 2 (CL_2), the length and area of the duct (DL, DA), and Piston area (PA) and the mechanical stiffness of the driver (K_m). The area of the stack is the same as the final area of cone 1, and the duct area is the same as the final area of cone 2. The piston area (PA) is equal to the initial area of cone 1. Among the design variables, the piston area (PA) and the mechanical stiffness of the driver (K_m) were used for electroacoustic efficiency optimization. All the other design variables were used for the second law efficiency optimization. Other driver parameters such as the resistance (R_e) and inductance (L_e) of the driver coil, force constant (Bl), mechanical resistance (R_m) and moving mass (M_m) were excluded from the design variables.

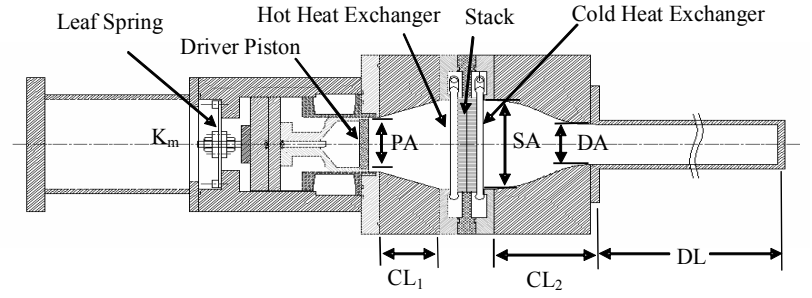

Figure 3: Design variables for Purdue prototype.

A 55% helium and 45% argon mixture was chosen. This mixture was found to be nearly optimal for the Purdue thermoacoustic cooler prototype (Mongeau *et al*., 2001). Viscous losses in the stack are reduced due the relatively low Prandtl number of this mixture (Swift, 2002). Heat exchanger dimensions were fixed. Key hardware such as the driver, the heat exchangers, and the stack porosity and solidity were therefore treated liked known fixed quantities, the focus of the optimization being on parameters that are possibly adjustable in experiments.

2.3 Guess and Target Vectors in DELTAE

Guess and target vectors are needed as input to DELTAE. Target vectors are boundary conditions or known values, and guess vectors are initial values required to perform the numerical integrations (Ward and Swift, 2001). Numerical integration of the wave and energy equations iteratively requires the determination of the guess vector values satisfying the given target vectors. Strategic choices for the guess vector values ensure numerical

convergence and accuracy. The target vectors used for this study include the hot-side and cold-side stack end temperatures, the acoustic power at the driver, the complex velocity at the termination end, and the total energy at the termination end. The acoustic power used was 10 W for Hofler's configuration, and 200 W for Purdue's configuration throughout the optimization. A zero phase angle between pressure and velocity was imposed at the driver, to ensure acoustic resonance. The guess vectors include the gas temperature at the driver, the operating frequency, the hot and cold side heat transfer rates, and the pressure at the driver. Insulated conditions downstream of the stack were imposed through the use of the segment "INSULATE" in DELTAE in order to consider the heat gain due to the dissipation of acoustic power in the cold-side heat exchanger.

3. RESULTS

3.1 Second Law Efficiency

For each temperature span, the design optimization program was used to yield the design to achieve the best second law efficiency. Optimal performance results for both the Hofler and the Purdue configurations are shown in Tables 1 and 2. The mean pressure used for the optimization was 3 MPa for both configurations. The hot-side stack end temperature was fixed to 300 K. The numerical results for the second law efficiency vs. the temperature difference across the stack were approximated using a second-order polynomial regression, to eliminate small random fluctuations. The root mean square errors of the regressions were 0.029 for Hofler's prototype and 0.034 for Purdue prototype. The regressions are shown in Fig. 4. The abscissa below the figure is the stack end temperature difference, and that above the figure is the absolute cold-side stack temperature. For a temperature span of 10 K, the optimal second law efficiency was about 30 % for Hofler's configurations, and 20 % for Purdue configuration. The optimal efficiency increased as the temperature span increased and reached a maximum of about 43 % and 38 % for Hofler's and Purdue's configurations, respectively, at the similar temperature lift value of 80 K (Tables 1 and 2). The efficiency finally then decreased to a value around 28 % and 22 % for Hofler's and Purdue's configurations, respectively, for a temperature span of 160 K. The largest second law efficiencies were achieved for temperature spans between 60 K and 100 K. This temperature span is typical of general purpose or low-temperature refrigeration. As can be seen Fig. 4, the best second law efficiency obtained from Hofler's configuration is larger than that obtained from the Purdue configuration. The slight increase in the maximum second law efficiency is partially due to the fact that Hofler's configuration (around one quarter wavelength long) is more compact and has less surface area than the Purdue (one half wavelength long) configuration, leading to less acoustic power dissipation (Swift, 2002).

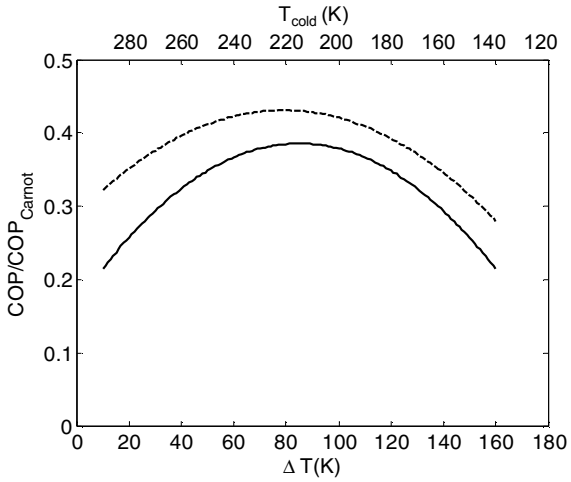

Figure 4: Second law efficiency vs. stack end temperature difference. ---: Hofler's prototype, — : Purdue prototype.

The optimized design variables are listed for both configurations in Tables 1 and 2. The stack length (*SL*) consistently increased with temperature span for both configurations. In general, a larger temperature span requires the use of a longer stack. Based on the change of the duct length (*DL*), the hot-side end of the stack moved towards the piston end as the temperature span increased. The area of the stack (*SA*) was relatively large when the cold-side stack end temperature was high, and decreased as the temperature was lowered. A relatively long and thin stack is thus needed to achieve low temperatures. A relatively short and thick stack is appropriate to achieve higher temperatures. Note that no bounds for the design variables were imposed. Therefore some of the values such as the

duct length, *DL*, are unreasonably large. This approach is useful to understand the major trends, i.e. how the second law efficiency behaves as the temperature span increases. To design a functional system, bounds on design variables can easily be imposed, leading to tradeoffs between performance and other design constraints.

Table 1: Optimized design variables for Hofler's prototype.

Tc(K)	DL_1(cm)	SA(cm^2)	SL(cm)	DA_2(cm^2)	DL_2(cm)	CL(cm)	CA(cm^2)	HV(cm^3)	PA(cm^2)	COPR	η_{dr}(%)
290	34.8	2757.8	5.4	313.0	153.8	6.5	155.9	2158900	2.49	0.304	85.7
280	27.2	1375.8	8.4	143.6	159.5	17.0	308.0	2869000	1.91	0.362	86.3
260	20.4	559.5	13.6	49.7	59.5	166.5	201.8	634160	1.46	0.412	86.0
240	15.1	319.2	17.4	30.9	142.9	42.5	335.8	295800	1.15	0.423	86.1
220	13.3	261.6	24.4	22.8	130.7	79.7	148.9	393010	1.00	0.426	88.1
200	10.7	244.3	30.3	17.1	114.4	159.2	178.6	626050	0.86	0.415	89.9
180	8.3	159.6	36.7	17.7	189.0	31.4	142.8	230210	0.75	0.384	89.8
160	6.1	116.4	41.3	8.5	53.6	589.2	305.3	84589	0.56	0.351	90.9
140	4.1	96.0	47.9	7.7	74.8	866.8	776.8	9716	0.49	0.283	91.7

Table 2: Optimized design variables for Hofler's prototype.

Tc(K)	SL(cm)	CL_1(cm)	SA(cm^2)	CL_2(cm)	CA(cm^2)	DL(cm)	K_m(kN/m)	PA(cm^2)	COPR	η_{dr}(%)
290	2.6	34.7	3105.7	0.8	487.0	128.0	908.21	58.86	0.197	60.5
280	3.5	23.6	2522.3	0.8	342.0	128.0	913.08	48.62	0.264	61.1
260	7.3	23.2	1653.9	1.4	461.6	249.4	335.65	44.70	0.347	61.0
240	8.7	13.7	1549.5	1.1	398.5	254.3	304.92	46.26	0.370	61.0
220	12.8	11.2	1119.2	1.7	310.1	278.7	233.01	40.30	0.378	61.0
200	16.9	7.2	914.6	1.7	283.4	293.4	194.38	41.50	0.368	61.0
180	19.4	3.9	859.8	1.6	293.4	321.2	153.29	37.67	0.343	61.0
160	22.2	1.2	810.2	1.4	290.1	337.0	126.22	34.42	0.297	61.0
140	25.7	0.2	731.5	1.2	293.8	338.2	110.67	29.44	0.218	61.0

3.2 Electroacoustic Efficiency

The optimal electroacoustic conversion efficiencies of the driver for both configurations are shown in the last column in Tables 1 and 2. For a given acoustic impedance, Z_a, at the driver piston, the electroacoustic conversion efficiency is a function of driver parameters such as the electrical resistance, R_e, the electrical inductance, L_e, the force constant, Bl, the mechanical stiffness, K_m, the mechanical moving mass, M_m, the mechanical resistance, R_m, and the piston area, PA (Wakeland, 2000, Paek *et al.*, 2005). Based on a linear electrical equivalent circuit model, the electroacoustic conversion efficiency is expressed as (Wakeland, 2000)

$$\frac{1}{\eta_{dr}} = \frac{R_e R_m}{(Bl)^2}\frac{R_m}{R_a}\left(1+\frac{R_a}{R_m}\right)^2 + \left(1+\frac{R_m}{R_a}\right) + \frac{R_e R_m}{(Bl)^2}\frac{X^2}{R_m R_a}, \tag{6}$$

where, R_a and X are

$$R_a = \mathrm{Re}\left[S^2 Z_a\right], \tag{7}$$

and

$$X = \mathrm{Im}\left[R_m + j\left(\omega M_m - \frac{K_m}{\omega}\right) + S^2 Z_a\right]. \tag{8}$$

In Eqs. (7) and (8), Re and Im represent the real part and the imaginary part, respectively, S is the area of the driver piston and ω is the angular frequency. X is the combined mechanical and acoustic reactance. Equation (6) can be written in another form (Paek *et al.*, 2005) as

$$\eta_{dr} = \frac{R_a (Bl)^2}{R_e\{X^2 + (R_m + R_a)^2\} + (Bl)^2 (R_a + R_m)}. \tag{9}$$

The maximum theoretical electroacoustic efficiency, which depends on only Bl, R_e and R_m, can be achieved when X is zero, and the other driver parameters satisfy (Wakeland, 2000)

$$\eta_{dr,\max} = \frac{\beta}{\beta + 2\sqrt{\beta + 1} + 2}, \tag{10}$$

where β is defined as (Wakeland, 2000)

$$\beta = \frac{Bl^2}{R_e R_m}. \tag{11}$$

For the Purdue configuration, Bl, R_e, and R_m are 9, 0.2, and 25, respectively, and the maximum theoretical electroacoustic efficiency was about 61.1 %. As seen in Table 2, the optimized electroacoustic conversion efficiencies for all the cases were close to the maximum value. The slightly low efficiency at 290 K may be due to an insufficiently small termination criterion for the cost function, $-\eta_{dr}$. A value of 1 % was used to reduce calculation time.

For Hofler's prototype, R_m and K_m were zero according to the original DELTAE model used for the prototype (Ward and Swift, 2001). This means that X in Eq. (6) or (9) is not zero but changes depending on the operating frequency and the acoustic impedance at the driver piston. In this case, the electroacoustic efficiency can be expressed based on Eq. (9),

$$\eta_{dr} = \frac{R_a Bl^2}{R_e (X^2 + R_a^2) + R_a Bl^2}. \tag{12}$$

Since the maximum theoretical electroacoustic efficiency for Hofler's configuration depends on the operating conditions, the optimized electroacoustic efficiencies are different for different temperatures.

3.3 Losses

The changes in second law efficiency are due to irreversibilities associated with the heat pumping process. The entropy generation for each temperature span was estimated from an entropy balance. For the overall thermoacoustic cycle, the entropy generation rate is given by

$$\dot{S}_{gen} = \frac{|\dot{Q}_h|}{T_h} - \frac{|\dot{Q}_c|}{T_c}, \tag{13}$$

where $\dot{S}_{gen}$ is the entropy generation rate, $\dot{Q}_h$ and $\dot{Q}_c$ are the hot and cold-side heat transfer rates and T_h and T_c are the hot and cold-side stack end temperatures. The entropy generation rates for the optimized results were calculated and are plotted in Fig. 5. The relationship between entropy generation rates and operating temperature are consistent with the second law efficiency for the given temperature spans. It reached a minimum when the temperature span was 80 K, where the second law efficiency was maximum.

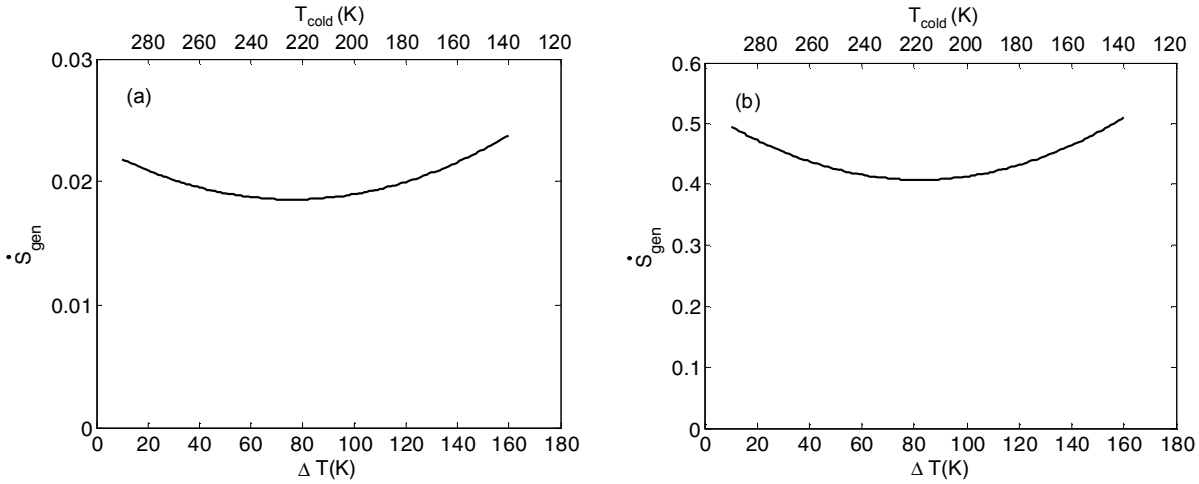

Figure 5: Entropy generation rate vs. stack end temperature difference. (a): Hofler's prototype, (b) Purdue Prototype.

The entropy generation was categorized in terms of two different types of losses based on their effects on the cooling power. $Loss_1$ is the acoustic power dissipation occurring in the segments between the stack and the driver. These directly reduce the useful acoustic power available for conversion to cooling power in the stack region. $Loss_2$ is the summation of the conduction in the stack and the acoustic power dissipated downstream of the stack in the resonator. These losses act as additional heat gain to the cold-side heat exchanger, and reduce the useful cooling power. A large portion of the acoustic power loss is converted to heat pumping power within the stack. It is difficult to separate the acoustic power absorbed for heat pumping from the acoustic power dissipated due to viscous and thermal losses. Therefore the absorbed power was not included in the analysis. Entropy generation due to finite temperature differences for heat transfer within the stack was not included. Although the analysis does not include all the losses, it is useful in understanding the relation between the second law efficiency and the temperature span.

Acoustic power dissipation in various segments was calculated in DELTAE based on (Swift, 2002)

$$\frac{d\dot{E}}{dx} = -\frac{r_v}{dx}\left|U_1\right|^2 - \frac{1}{2r_\kappa}\left|p_1\right|^2, \tag{14}$$

where $\dot{E}$ is the dissipated acoustic power, r_v is the viscous resistance per unit length, and r_κ is the thermal-relaxation conductance per unit length. The conduction loss, $\dot{W}_{cond}$, in the stack region can be approximately calculated by

$$\dot{W}_{cond} = (A_{gas}k_{gas} + A_{s\,olid}k_{solid})\frac{T_c - T_h}{SL}, \tag{15}$$

where T_c and T_h are the cold-side and hot-side stack end temperature, respectively, A is the area, k is the thermal conductivity and SL is the stack length. The subscripts, "gas" and "solid" represent the gas mixture and the stack material, respectively. Thermal conductivities in Eq. (15) are average values for the hot-end and the cold-end of the stack.

Table 3: Losses associated with DELTAE for Hofler's prototype.

Tc(K)	Loss I(W)	Loss II(W)	$\dot{W}_{ac}$ (W)	$\dot{Q}_c$ (W)	Loss I/ $\dot{W}_{ac}$	Loss II / $\dot{Q}_c$	COP	COPcarnot	COPR
290	1.72	6.28	10	90.19	0.172	0.070	9.02	29.67	0.304
280	1.35	4.33	10	51.38	0.135	0.084	5.14	14.19	0.362
260	1.02	2.56	10	27.06	0.102	0.095	2.71	6.57	0.412
240	0.87	1.88	10	17.05	0.087	0.110	1.70	4.03	0.423
220	0.68	1.46	10	11.80	0.068	0.123	1.18	2.77	0.426
200	0.57	1.28	10	8.35	0.057	0.154	0.83	2.01	0.415
180	0.49	0.94	10	5.79	0.049	0.163	0.58	1.51	0.384
160	0.46	0.79	10	4.03	0.046	0.197	0.40	1.15	0.351
140	0.40	0.66	10	2.49	0.040	0.266	0.25	0.88	0.283

Table 4: Losses associated DELTAE for Purdue prototype.

Tc(K)	Loss I(W)	Loss II(W)	$\dot{W}_{ac}$ (W)	$\dot{Q}_c$ (W)	Loss I/ $\dot{W}_{ac}$	Loss II / $\dot{Q}_c$	COP	COPcarnot	COPR
290	32.42	58.38	200	1284.53	0.162	0.045	6.42	32.60	0.197
280	29.58	55.42	200	780.58	0.148	0.071	3.90	14.78	0.264
260	23.43	40.56	200	463.22	0.117	0.088	2.32	6.67	0.347
240	22.16	30.70	200	301.10	0.111	0.102	1.51	4.07	0.370
220	17.54	23.03	200	211.20	0.088	0.109	1.06	2.79	0.378
200	14.89	19.05	200	149.05	0.074	0.128	0.75	2.03	0.368
180	14.98	18.98	200	104.13	0.075	0.182	0.52	1.52	0.343
160	15.05	18.81	200	68.78	0.075	0.274	0.34	1.16	0.297
140	15.07	18.34	200	38.62	0.075	0.475	0.19	0.89	0.218

Tables 3 and 4 show losses estimated for both prototypes. In both cases, the ratio of $Loss_1$ to acoustic power is high when the temperature span is small, and gets smaller as the temperature span increases. The explanation for this behavior is related to the fact that larger temperature spans require longer stacks (see Tables 1 and 2) and result in

greater viscous losses. In order to reduce these losses, the optimal design involves moving the stack closer to the velocity node at the driver (see Tables 1 and 2) with increasing temperature span. This reduces viscous losses in the region between the driver and stack.

On the other hand, the ratio of $Loss_2$ to the cooling power is small when the temperature span is small and increases as the temperature span is increased. This is because conduction within the stack increases with increasing temperature difference, and viscous losses increase due to the requirement for a longer cold duct section.

3.4 Comparison with Experimental Results

The optimization results were compared with the measured performances of various previously built thermoacoustic coolers. The second law efficiencies of the various thermoacoustic coolers are listed in Table 5 for operating conditions close to their design values.

Table 5: Various thermoacoustic cooler performances

Name	ΔT(°C)	Tc(°C)	$\dot{Q}_c$ (W)	COPR
Prototype at Purdue (Paek, 2005)	8.9	15.6	40	0.033
Frankenfridge (Poese and Garrett, 2000)	10.8	17.2	26	0.067
Triton (Garrett, 2002)	18	10.4	2161	0.04
Solar powered TAC (Adeff and Hofler, 2000)	26	1.3	5	0.16
Portable TAC (Berhow, 1994)	35	0	10	0.13
SETAC (Ballister and McKelvey, 1995)	39.5	-1.3	294	0.26
Tijani's cooler (Tijani, 2001)	45	-29	4	0.11
Ben and Jerry Cooler (Garrett, 2002)	58.5	-24.6	119	0.22
Hofler's cooler (Hofler, 1996)	66	-39	1.7	0.16

The results indicate that the second law efficiencies of coolers having relatively small temperature spans consistent with air-conditioning applications were small. They were larger for those having relatively large temperature spans representative of refrigeration applications. The best second law efficiency achieved so far experimentally has been 26 % for the SETAC prototype.

The second law efficiencies from the optimization program and actual thermoacoustic cooler data are plotted in terms of the temperature span and the cold-side stack end temperature in Fig. 6. Although the simulation results span a wider range of operating temperatures, the trends are similar within the range of the experimental data. From a performance perspective, thermoacoustic cooling is less efficient for applications with either low or high temperature spans such as air conditioning or cryogenic cooler than for operating conditions associated with refrigeration.

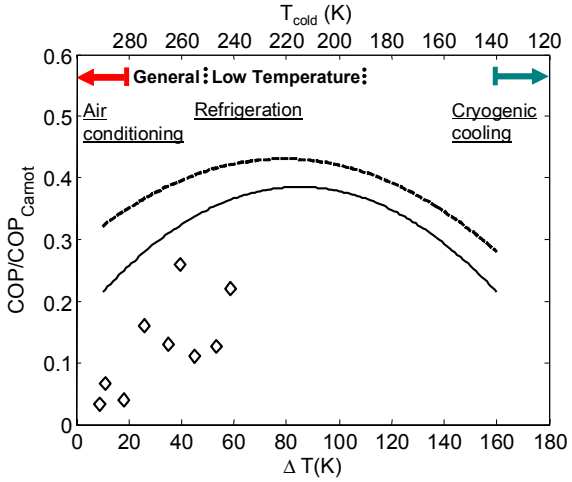

Figure 6: Second law efficiency vs. stack end temperature difference. ---: from Hofler's prototype, — : from Purdue prototype, ◊: from various cooler performances listed in Table 5.

4. CONCLUSIONS

A simple design optimization tool was developed for thermoacoustic coolers and applied to evaluate the best second law efficiencies for two different prototype configurations for a range of different operating conditions. It was found that maximum second law efficiency occurs for a temperature difference between the hot and cold ends of the system of about 80 K. A similar trend of increasing second law efficiency with temperature span below 80 K was found when looking at the results from experiments that have been performed on a range of different prototype thermoacoustic coolers that have been reported in the literature. From a performance perspective, thermoacoustic cooling seems to make less sense for applications with either low or high temperature spans such as air conditioning or cryogenic cooling than for operating conditions associated with refrigeration. This conclusion is useful for targeting appropriate applications that should be investigated for thermoacoustic cooling.

REFERENCES

Adeff, A., and Hofler, T.J., 2000, Design and construction of a solar-powered, thermoacoustically driven, thermoacoustic refrigerator, *J. Acoust. Soc. Am.*, vol. 107, issue 5: p. L37-L42.

Ballister, S.C., and McKelvey, D.J., 1995, *Shipboard electronics thermoacoustic cooler*, Master's Thesis, Physics Department, Naval Postgraduate School, Monterey, CA, 102 p.

Berhow, T.J., 1994, *Construction and performance measurement of a portable thermoacoustic refrigerator demonstration apparatus*, Master's thesis, Physics department, Naval Postgraduate School, Monterey, CA, 81p.

Garrett, S. L., 2002, Next-generation thermal management, Slides used for Presentation, Dallas/Ft. Worth, Texas.

Hofler, T.J., 1986, *Thermoacoustic refrigerator design and performance*, Ph.D. dissertation, Physics department, University of California, San Diego, CA, 142 p.

Mathews, J.H., and Fink, K.D., 1998, *Numerical methods using MATLAB*, Prentice Hall, New Jersey, 662 p.

Minner, B.L., Braun, J.E., and Mongeau, L., 1997, Theoretical evaluation of the optimal performance of a thermoacoustic refrigerator, ASHRAE transactions, vol. 103, part 1: p. 873-887.

Mongeau, L., Alexander, A., Minner, B. L., Paek, I., and Braun, J.E., 2001, Experimental investigations of an electro-dynamically driven thermoacoustic cooler, *Proceedings of the 2001 International Mechanical Engineering Congress and Exposition*, ASME: p. 1-12.

Moran, M.J., and Shapiro, H.N., 2000, Fundamentals of engineering thermodynamics, Wiley, New York, 918 p.

Nelder, J.A., and Mead, R., 1965, A simplex method for function minimization, *Computer Journal*, vol. 7, p. 308-313.

Paek, I., 2005, *Characterization of thermoacoustic cooler components and systems*, Ph. D. dissertation, School of Mechanical Engineering, Purdue University, West Lafayette, IN, 123 p.

Paek, I., Mongeau, L., and Braun, J.E., 2005, A method for estimating the parameters of electrodynamic drivers in thermoacoustic coolers, *J. Acoust. Soc. Am.*, vol. 117, issue 1: p. 185-193.

Poese, M.E., and Garrett, S.L., 2000, Performance measurements on a thermoacoustic refrigerator driven at high amplitudes, *J. Acoust. Soc. Am.*, vol: 107, issue 5: p. 2480-2486.

Swift, G.W., 2002, *Thermoacoustics: A unifying perspective for some engines and refrigerators*, Acoustical Society of America, New York, NY, 300 p.

Tijani, M.E.H., 2001, *Loudspeaker-driven thermo-acoustic refrigeration*, Ph. D. dissertation, Technische Universiteit Eindhoven, Eindhoven, 170 p.

Tijani, M.E.H., Zeegers, J.C.H., and Waele, A.T.A.M., 2002, The optimal stack spacing for thermoacoustic refrigeration, *J. Acoust. Soc. Am.*, vol. 112, issue 1: p. 128-133.

Tijani, M.E.H., Zeegers, J.C.H., and Waele, A.T.A.M., 2002, Prandtl number and thermoacoustic refrigerators, *J. Acoust. Soc. Am.*, vol. 112, issue 1: p. 134-143.

Wakeland, R.W., 2000, Use of electrodynamic drivers in thermoacoustic refrigerators, *J. Acoust. Soc. Am.*, vol. 107, issue 2: p. 827-832.

Ward, W.C., and Swift, G.W., 1994, Design environment for low-amplitude thermoacoustic engines (DeltaE), J. Acoust. Soc. Am., vol. 95, issue 6: p. 3671-3672.

Ward, W.C., and Swift, G.W, 2001, *DELTAE Tutorial and User's Guide Version 5.1*, Los Alamos National Laboratory, Los Alamos, NM, 166 p. Software and user's guide are available online at http://www.lanl.gov/thermoacoustics/doc-options.html.

Wetzel, M., and Herman, C., 1997, Design optimization of thermoacoustic refrigerators, *Int. J. Refrig.*, vol. 20, issue 1: p. 3-21.